



Overview of optical coherence tomography in neuro-ophthalmology

Emanuel R. de Carvalho^{1,2}, Peter M. Maloca^{1,3,4,5}

¹Moorfields Eye Hospital NHS Foundation Trust, London, UK; ²Department of Ophthalmology, University Medical Center Amsterdam, University of Amsterdam, Amsterdam, The Netherlands; ³Institute of Molecular and Clinical Ophthalmology Basel (IOB), Basel, Switzerland; ⁴OCTlab, Department of Ophthalmology, University Hospital Basel, Basel, Switzerland; ⁵Department of Ophthalmology, University of Basel, Basel, Switzerland

Contributions: (I) Conception and design: All authors; (II) Administrative support: All authors; (III) Provision of study materials or patients: All authors; (IV) Collection and assembly of data: All authors; (V) Data analysis and interpretation: All authors; (VI) Manuscript writing: All authors; (VII) Final approval of manuscript: All authors.

Correspondence to: Emanuel R. de Carvalho. Moorfields Eye Hospital NHS Foundation Trust, 162 City Road, London EC1V 2PD, UK.

Email: e.decarvalho@nhs.net.

Abstract: Optical coherence tomography (OCT) is a widely used non-invasive medical imaging technology that has revolutionized clinical care in ophthalmology. New developments, such as OCT angiography (OCTA) are expected to contribute even further to the widespread use of OCT-based imaging devices in the diagnosis and monitoring of patients with ophthalmic diseases. In recent years, many of the disadvantages such as limited field of view and imaging artefacts have been substantially reduced. Similar to the progress achieved in the assessment of retinal disorders, OCT is expected to change the approach to patients seen in the neuro-ophthalmology clinic. In this article, we review the technical features of OCT and OCT-based imaging techniques, highlighting the specific factors that should be taken into account when interpreting OCT in the field of neuro-ophthalmology.

Keywords: Optic disc; optical coherence tomography (OCT); angiography; retina; macula; neuro-ophthalmology; volume rendering; virtual reality

Received: 13 September 2019; Accepted: 19 December 2019; Published: 15 June 2020.

doi: 10.21037/aes.2019.12.08

View this article at: <http://dx.doi.org/10.21037/aes.2019.12.08>

Introduction

Optical coherence tomography (OCT) is characterized by the use of low-coherence interferometry to obtain micrometer-resolution cross-sectional images from within living tissue (1,2). The lateral resolution depends on the spot size of the light beam and the depth resolution (or axial resolution) depends mainly on the optical bandwidth of the light source (3). In recent years, two main variants have been developed: spectral-domain OCT (SD-OCT) and swept-source OCT (SS-OCT). In both systems, the reference arm length is fixed, and the depth information of the reflected signal is analyzed with a spectrometer using a Fourier transformation. In SD-OCT, the light

source is emitted mostly below 100 kHz A-scans/s in the visible infrared range (~800 nm), whereas SS-OCT uses invisible light to the human eye (~1,000 nm), up to an ultramegahertz sample speed (4). Novel imaging modalities have improved the visualization of the retina and the choroid using enhanced depth imaging OCT (EDI-OCT), which is acquired by placing the OCT device closer to the eyes producing an inverted mirror image of the retina and placing the outer choroid in closer proximity to the zero-delay line. This improves choroidal visualization as the choroid, compared with standard OCT, is characterized by a lower frequency portion on the Fourier-transformed interferogram (5,6). Choroidal thickness measurements by EDI-OCT provided new insights into the changes of

choroidal thickness between individuals which was shown to depend on age, refractive index, and axial length (7-9). Recently, OCT angiography (OCTA) was introduced as an OCT-based technique capable of assessing the retinal and choroidal vascular network and blood flow (10,11). This technique is evolving at a fast pace as exemplified by the description of new OCT image display techniques such as volume rendering and virtual reality image display (*Figure 1*) (12-16).

The introduction of OCT and OCT-based imaging techniques has already led to major developments in the understanding of a myriad of neuro-ophthalmic disorders, facilitating clinical diagnosis and monitoring (*Video 1*). In the future, OCT is expected to serve as a highly reliable, non-invasive biomarker for neurodegeneration and axonal damage in multiple sclerosis (MS) (17). It is therefore of paramount importance that clinicians are familiar with the advantages and limitations of OCT in the assessment of the patient presenting to the neuro-ophthalmology clinic and that interpretation of findings takes into account the clinical presentation and all factors that can affect image acquisition and display.

Interpretation of the OCT image in neuro-ophthalmology

Optic nerve head (ONH)

Imaging of the ONH can be performed in both two and three dimensions (2D and 3D) using numerous protocols. It is important to always repeat the same method in the course of follow-up to enable longitudinal conclusions. The radial 2D scan is composed from a number of cross-sections centered at the level of the ONH at equal angular orientation. Correct positioning of the scan is important because otherwise incorrect measurements can easily be generated. The 3D volumetric cube is obtained by raster scanning of a square centered on the ONH enabling the display of any slice of the cube of data acquired in the scan. *Figure 2* displays the normal findings in a healthy subject with a minor cupping compared to a patient with optic disc drusen (ODD). The retinal nerve fiber layer (RNFL) exhibits a directional hyperreflectance, increasing in thickness as it approaches the margin of the ONH. The signal reflected from the RNFL decreases at the level of the disc rim, because as the nerve fibres blend into the ONH, they are no longer perpendicular to the incident OCT optical beam. The RNFL covers a relative hyporeflexive

area of the ganglion cell layer (GCL) mostly visible towards the macula. Due to the relatively high density of nuclei, the inner plexiform layer (IPL) and outer plexiform layer (OPL) are moderately reflective, while the inner nuclear layer (INL) and ONL are weakly reflective. The inner segment (IS) and outer segment zone (OS) is visible as a thin, highly backscattering line immediately anterior to the retinal pigment epithelium (RPE) which is visible as a highly backscattering layer that abruptly terminates at the margin of the disc. The choriocapillaris is represented as a hyporeflexive area which in healthy eyes is directly adjacent to the RPE. The RPE terminates at the margin of the optic nerve head and is commonly used as a landmark.

When interpreting OCT images, it is important to note that the images are often axially stretched on the computer display in order to improve the visualization of the different retinal layers. The depth of the optic disc cup is thus exaggerated. Quantitative morphometry of the images using the correct axial and transverse scales is advised.

Structural OCT scans of the ONH are useful in the assessment of lesions of the optic nerve, such as ODD and peripapillary hyperreflective ovoid mass-like structures (PHOMS), optic nerve hypoplasia, optic nerve tumors, myelinated retinal nerve fibres, amongst others.

EDI-OCT should be used when analyzing the deeper structure of the ONH, given that several features are missed when using SD-OCT only. EDI-OCT captures the entire ONH to the level of the lamina cribrosa and has been shown to possess improved diagnostic accuracy in identifying structural lesions of the ONH when compared to ultrasound (18).

Assessment and diagnosis of ODD is one of the most common indications for EDI-OCT of the ONH. The guidelines for the assessment of ODD, published by the Optic Disc Drusen Studies Consortium, include the use of EDI-OCT of the ONH, alongside evaluation of the RNFL, the macula (to assess for macular edema secondary to papilledema), and autofluorescence (19). Drusen appear as “discrete lump-like” hyporeflexive areas surrounded by hyperreflective borders or collections of hyperreflectivity without the core (*Figure 2C*) (20,21). The hyperreflective signal surrounding the hypoechoic area is referred as the “cap” sign as the signal does not penetrate deep enough to capture the core of the drusen (20,21). Blood vessels, which appear as elongated tube-like structures, are distinguished as they lack this hyperreflective signal around them. Besides the clinical classification of buried versus superficial drusen, Traber *et al.*

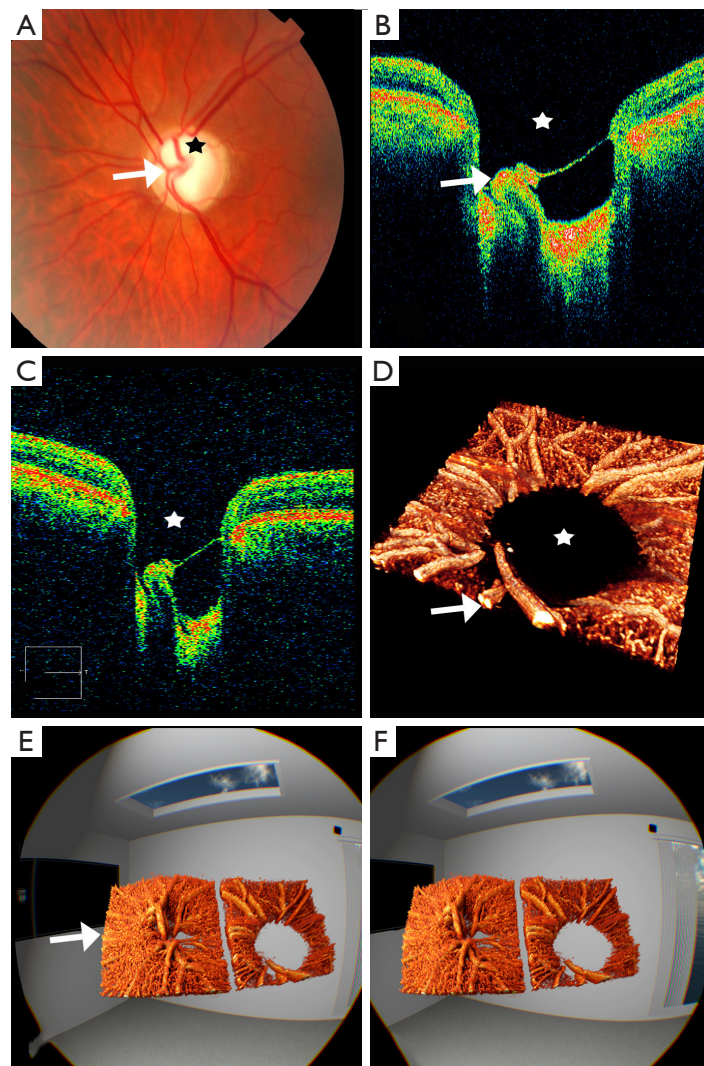


Figure 1 Evolution of OCT imaging and display technology representing the left eye in a glaucoma patient over 15 years follow-up. (A) Traditional color fundus imaging shows a pale optic disc, with a large excavation (black star) and displacement of the vascular tree (arrow); (B) stratus time-domain OCT (radial lines, scan length 4 mm) representing the distinct depth of the excavation (white star). The RNFL is hardly recognizable and the vessels next to the lamina cribrosa are displaced due to tissue loss; (C) spectral domain OCT (Cirrus OCT 5000, 200×200 pixel) corresponding to the findings in (B). An improved depiction of retinal layers and lamina cribrosa can be appreciated; (D) volume rendered SD-OCT angiography complements the previous structural OCT technology by displaying the flow within the vessels. Inside the optic disc, the vessels' void area (secondary to tissue atrophy, white star) is shown; (E,F) novel interactive display of OCTA information using virtual reality technology shown in stereoscopic image illustration. The conventional computer screen for image display has been discarded and the user is immersed directly into the original OCTA volume data. On the left side the numerous optic disc vessels of a healthy subject are shown with a raised vessel tree (white arrow). In contrast, the aforementioned glaucoma patient (right) shows a heavily rarefied vessel architecture with preservation of only the larger vessel calibers. Profound OCTA vessel deficiency in the central optic disc area is visualized. Both images can be fused for a 3D impression. OCT, optical coherence tomography; RNFL, retinal nerve fiber layer; SD-OCT, spectral-domain OCT; OCTA, optical coherence tomography angiography.

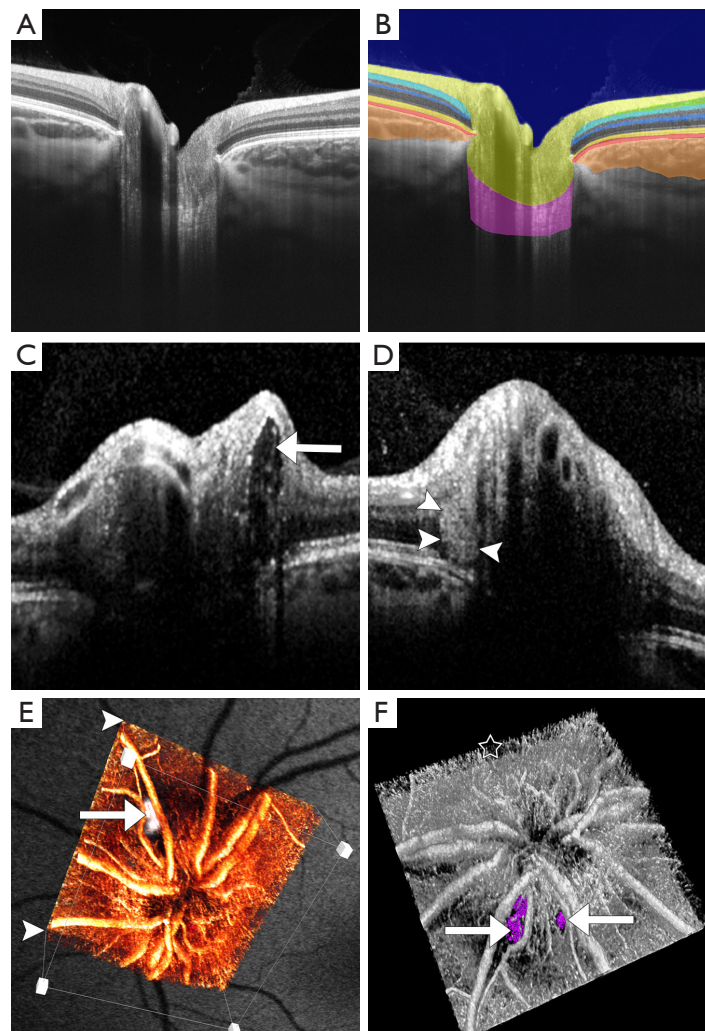


Figure 2 OCT imaging of a normal optic disc and in a case with superficial ODD in an asymptomatic 58-year-old female. (A) Swept source cross-sectional OCT depicts a normal optic disc (OD) with a minor excavation; (B) corresponding colored image display of the same OD as in (A). The vitreous is highlighted in blue. The RNFL is segmented in yellow crossing the lamina cribrosa (in violet). The ganglion cell layer is only detectable towards the macula (green). The inner and outer hyperreflective plexiform layers are shown in light and dark blue, respectively. The hyporeflective inner and outer nuclear layer were not segmented. The inner segment (IS) and outer segment (OS) zone is visible as a thin zone (gold), which lies close to the thin RPE (red). The choroid is outlined as a broad layer ending at the optic disc border (orange); (C) the ODD is characterized by a hyporeflective core surrounded by a hyperreflective signal (arrow); (D) EDI-OCT imaging of PHOMS in an asymptomatic 23-year-old female. The lesions are located in the peripapillary zone and are defined by moderate hyperreflectivity without defined margins (arrowheads); (E) correlation of autofluorescence imaging of superficial ODD (arrow) from another patient and advanced volume rendered OCTA imaging (arrowheads); (F) combined 3D OCTA and segmented superficial drusen from the same eye as in (E). Enhanced 3D imaging displays spatial interweaving of two drusen (arrows), which causes a decrease and narrowing of the vessels (asterisk). OCT, optical coherence tomography; ODD, optic disc drusen; RNFL, retinal nerve fiber layer; EDI-OCT, Enhanced-depth imaging optical coherence tomography; PHOMS, peripapillary hyperreflective ovoid mass-like structures; OCTA, optical coherence tomography angiography.

identified three OCT morphologic types, peripapillary ODD, granular ODD and confluent ODD (22). Confluent ODD appears hyporeflective and is associated with worse mean deviation scores on visual fields (22). It has subsequently been shown that the structures labelled as peripapillary ODD in the study by Traber *et al.* are not actually ODD but PHOMS (Figure 2D).

The etiology of PHOMS has not been elucidated, but appears to be distinct from traditional ODD based on their imaging features. They are located in the immediate peripapillary zone, appear hyperreflective, do not have clearly defined margins and lack a hyporeflective core (19). They are neither captured by ultrasound or autofluorescence and appear in patients irrespective of the presence of ODD or papilledema (23).

In papilledema, assessment of the peripapillary RNFL (pRNFL), which is described in the next sub-chapter, can aid in the differentiation of mild papilledema versus pseudopapilledema (e.g., secondary to ODD). From a structural point of view, on EDI-OCT, the pRNFL in papilledema appears swollen, often leading to the disappearance of the normal cupping of the disc. Caution should be exerted when assessing the RNFL in patients with congenital crowded optic discs as the difference between RNFL measurements has not been found to be statistically significant (24).

In ONH sheath meningioma, the peripapillary RPE—Bruch's membrane complex surrounding the optic canal opening becomes indented, creating an inverted U-shape deformation directed at the vitreous that presumably reflects the shape of the underlying load-bearing peripapillary sclera. In healthy subjects the peripapillary RPE—Bruch's membrane layer bordering the optic canal creates a V-shape, pointing away from the vitreous (25).

In optic nerve hypoplasia, OCT scans through the ONH showed significantly smaller horizontal disc diameters, horizontal cup diameters, and cup depths compared with the unaffected eyes and eyes of healthy controls, highlighting the reliability of OCT as a diagnostic tool (26). OCT can also be used to differentiate between optic disc melanoma or other infiltrative lesions and the relatively benign optic disc melanocytoma. In the latter, the mass usually shows a hyperreflective surface with smooth moderately reflective internal architecture and dense posterior optical shadow. Importantly, the choroidal and outer retinal architecture are preserved (27). In cases of myelinated RNFL, OCT reveals significant hyperreflectivity and increased thickness of the RNFL in the area of myelinated fibers (28-30).

Macular imaging

The introduction of OCT for the assessment and visualization of the retina and choroid has had a tremendous impact in the field of retinal diseases. Sampling of the macula allows the visualization of all retinal layers and choroid, reminiscent of an *in vivo* tissue biopsy. The macula can be scanned by 3D cube, line and cross-line, raster, mesh and radial scan patterns. Line scans, commonly used in clinic, are obtained by the averaging of multiple scans at a similar location, typically performed along a single location or along several parallel lines. Mesh scan patterns include information stemming from both horizontal and vertical orientations. A relatively long temporal gap between adjacent points perpendicular to the scan orientation is present, irrespective of the scanning rate, leading to image distortion along the slow axis of the scan. Simultaneous registration of the horizontal and vertical scans improves the quality of the scan by minimizing the distortion in the slow axis. Radial scans acquire multiple evenly spaced linear scans intersecting at the fovea, providing information from the macular region, with increased coverage at the line intersection (fovea), and decreased coverage near the periphery of the macula. In radial scanning, the interspaces have to be interpolated peripherally, but a major advantage lies in the fact that the information density is accentuated towards the center.

RNFL

Assessment of the pRNFL thickness is one of the most commonly used parameters in ophthalmology. This measure represents the quantification of the axons of the retinal ganglion cells that travel from the retina and form the ONH. For this reason, changes in RNFL thickness represent a structural marker of axonal integrity in many pathological processes involving the optic nerve. This measurement is calculated from a circle centered on the ONH with a diameter of 3.4 mm. Misplacement of the circle during repetitive scanning will result in increased measurement variability and erroneous measurements. The RNFL thickness may also be extracted from the 3D cube scanning pattern, allowing repositioning of the circle if necessary, and ensuring consistent tissue sampling location through multiple scans. In OCT, the RNFL is visualized as a highly backscattering layer at the vitreoretinal interface. The image-processing methods required for RNFL thickness measurements must be relatively insensitive to changes in morphology and signal intensity. The

anterior boundary is defined at the vitreoretinal interface. The posterior boundary is determined as the detection algorithm is moved backward to identify the second point of increased signal intensity after identification of the second highly reflected layer which is defined by the photoreceptors and RPE. Adjacent A-scans assist in the detection of the boundaries. Segmentation of the RNFL is more sensitive to OCT image quality variations than the total retinal thickness measurements, warranting caution in interpretation of the findings put forward by automated segmentation. SD-OCT devices record the average pRNFL thickness measurements in four quadrants (temporal, superior, nasal and inferior) and sectoral thicknesses at each of the 12 clock-hours or in 16 equal sectors. The ISNT rule (inferior > superior > nasal > temporal) is followed, whereby the inferior quadrant possesses the thickest RNFL, followed by superior, nasal and temporal quadrants. Other devices display the RNFL thickness as a color-coded thickness map of the entire peripapillary region, which can be useful in the assessment of small, localized areas of thinning outside the sampling location.

Figure 3 shows the pRNFL scans obtained with the Spectralis OCT, where the RNFL thickness is measured by assessing a total of 2,324 data points along the sampling circle. The built-in software constructs the final cross-section by averaging 16 consecutive B-scans. The averaging of multiple scans reduces the background noise and improves the quality of the signal. The report displays global average thickness, thickness in four quadrants and thickness in six sectors. With the Cirrus HD-OCT system, the deviation map compares the RNFL measurements at each super-pixel with an age-matched normative database, and locations under the lower 95% of the normal range are signalled. Quantitative ONH parameters are provided in the center panel of the scan report, with color-coding reflecting the comparison with the age-matched normative database (green depicts average measurements within normal limits; yellow depicts average measurements within borderline limits and red represents average measurements outside borderline limits). Normal RNFL thickness is approximately 105 μm with an estimated physiological loss due to aging of about 0.017% per year from age 18 onwards, translating in a 10- to 20- μm loss over a period of 60 years (31).

Ganglion cell—IPL thickness measurement and analysis

The inner retinal complex is defined as the combination of

RNFL, GCL and IPL. In 1963, van Buren described the development of retrograde trans-synaptic degeneration incurred as a reaction to damage of the post-geniculate afferent visual pathways (32). OCT segmentation measurements of GCL thinning with subtle changes of the INL provide a quantifiable measurement of pre-geniculate visual pathway dysfunction, and may provide an indirect visualization of retrograde trans-synaptic degeneration *in vivo* (33-35). Cirrus HD-OCT extracts the information from an ellipse (vertical radius of 2 mm, horizontal radius of 2.4 mm) centered on the fovea, providing a combined measurement that includes the GCL layer and the IPL. RTVue (Optovue, Fremont, US) segments the GCL complex that includes the macular RNFL, GCL and IPL layer. The data is captured from a 7-mm² area centered 1 mm temporal to the fovea. Spectralis SD-OCT (Heidelberg Engineering, Heidelberg, Germany) measures the GCL layer via automated segmentation of perifoveal volumetric retinal scans, usually comprising high resolution 20° × 5° volume scans (49 B-scans 30 microns apart, 1,024 A scans). Imaging quality is improved by automatic real time (ART), a setting that reduces noise by averaging multiple B-scans and an eye-tracking modality, Tru-Track, which improves the reproducibility of the scan. Repeatability and reproducibility of automated total retinal thickness measurements using SD-OCT has been demonstrated in healthy individuals as well as those with ocular disorders (36). Compared to other OCT instruments, the Spectralis SD-OCT presents the highest reproducibility of automated crude central foveal thickness measurement (*Figures 4-6*) (37).

The most sensitive early indicator of early damage to the anterior visual pathways is the assessment of the macular ganglion cell inner plexiform layer (mGCIPL). This is especially useful when assessing patients with optic neuropathies, both in the acute and chronic stages and disorders of the anterior visual pathways. Ganglion cell loss has been reported to occur 6 weeks after the initial insult in most cases (38). Thickness measurements of the mGCIPL have been found to correlate better with structure and function and the area of presenting visual field loss, at least in part due the superior reproducibility of GCIPL over RNFL thickness measurements (39,40).

In cases where optic disc edema is seen at onset, such as in ischemic optic neuropathies and optic neuritis, the loss of RNFL is masked by disc swelling, rendering mGCIPL a more reliable indicator of early damage. More specifically, in ischemic optic neuropathy, the thinning of mGCIPL has been shown to occur as early as 2.2 days after onset

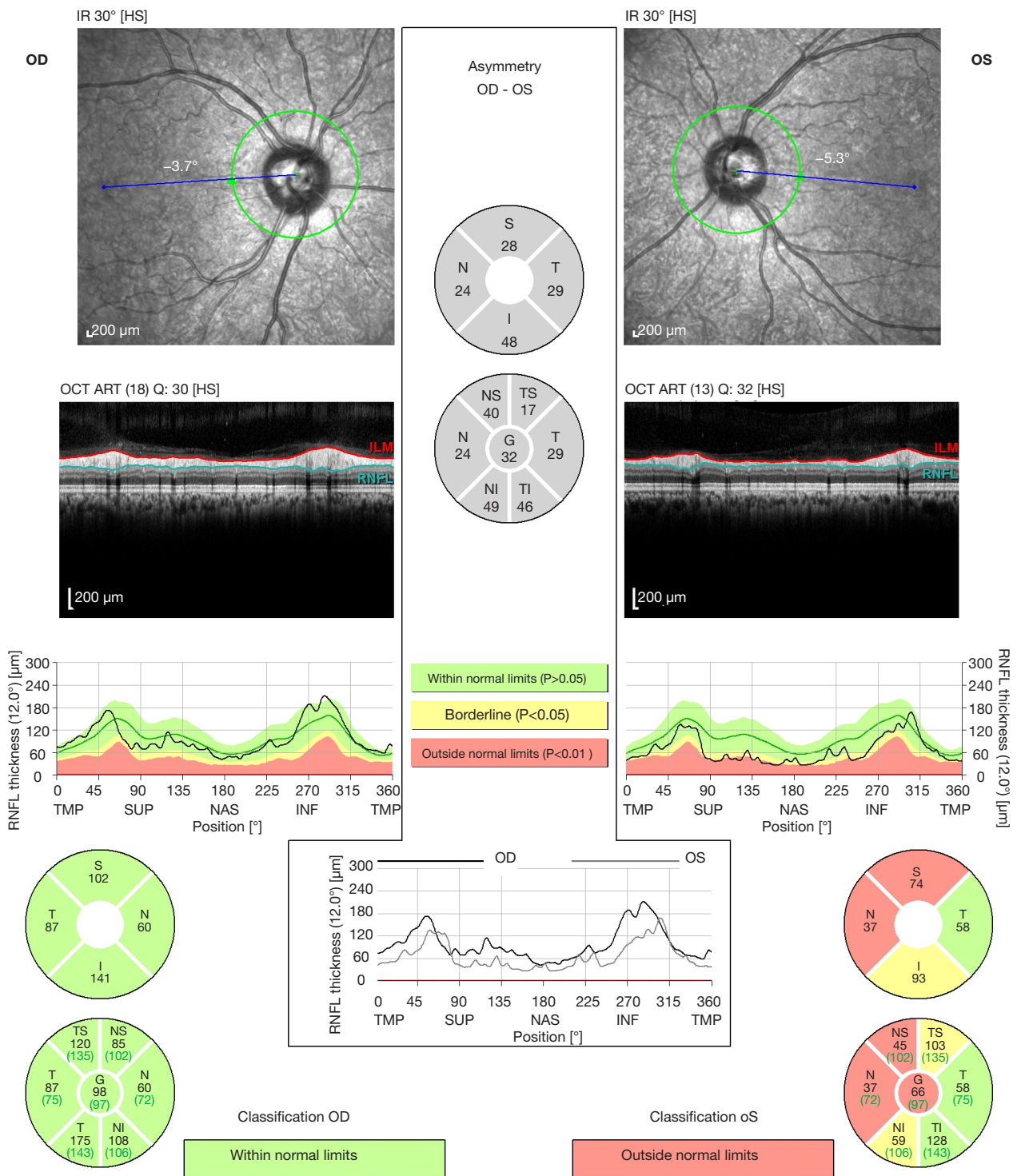


Figure 3 SD-OCT RNFL exam report in a 66-year-old male with left compressive optic neuropathy. Supero-nasal RNFL thinning is present in the left eye, correlating with the visual field deficit. OD, right eye; OS, left eye; RNFL, retinal nerve fibre layer; SD-OCT, Spectral-domain optical coherence tomography.

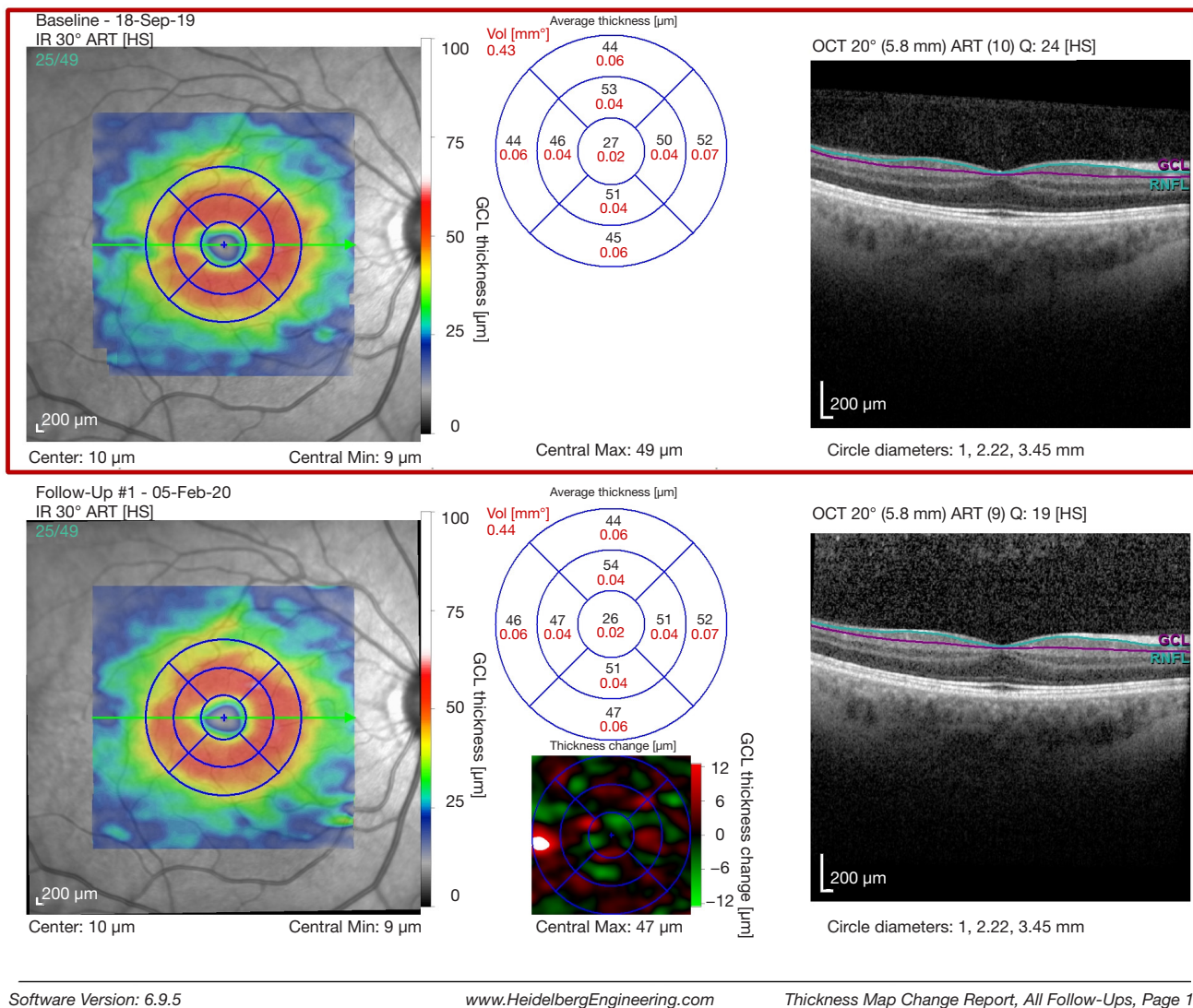
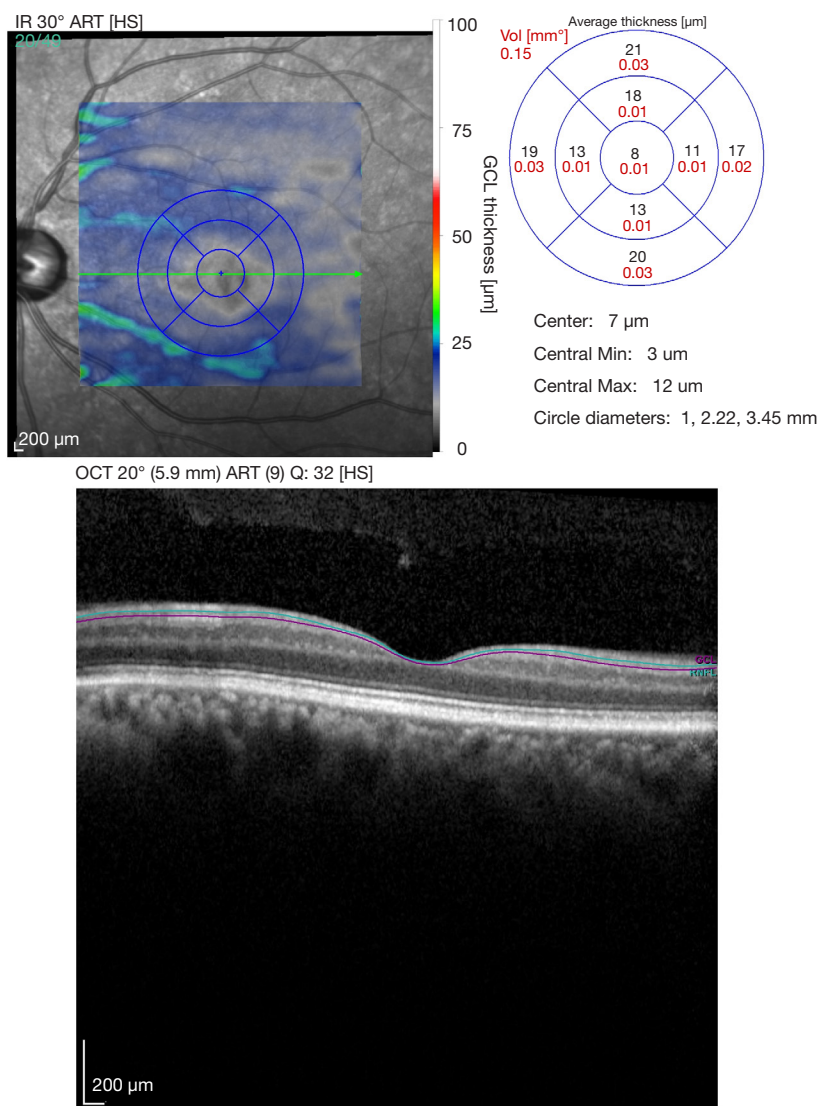


Figure 4 Display software of serial mGCL density SD-OCT segmentation analysis (1, 2.22, 3.45 mm volume scan) in a healthy, asymptomatic patient. The average volume change shows no significant change in mGCL density. mGCL, Macular ganglion cell layer; SD-OCT, spectral-domain optical coherence tomography.

of symptoms, whereas the mGCIPL map was abnormally thinner in 62.5% of eyes at presentation (41). In 2017, Petzold *et al.* (35) performed a meta-analysis of available published reports on OCT in patients with MS and found thinning of the pRNFL in eyes with a history of acute optic neuritis secondary to MS (MSON) (mean difference 20.1 μm) and in eyes without a history of acute optic neuritis secondary to MS (MSNON) (mean difference 7.41 μm , 8.98 to 5.83; $P < 0.0001$). In patients with a history of acute

optic neuritis secondary to MS, mGCIPL was 16.42 μm for MSON eyes and -6.31 μm for MSNON eyes compared with control eyes. These results correlate directly with the earlier meta-analysis that described thinning of the pRNFL in MSON eyes (35,42). As expected, no statistical difference in the thickness of the combined outer nuclear layer and OPL was observed when comparing MSON and MSNON with healthy eyes.

As previously mentioned, the pattern of mGCIPL loss



Software Version: 6.9.5

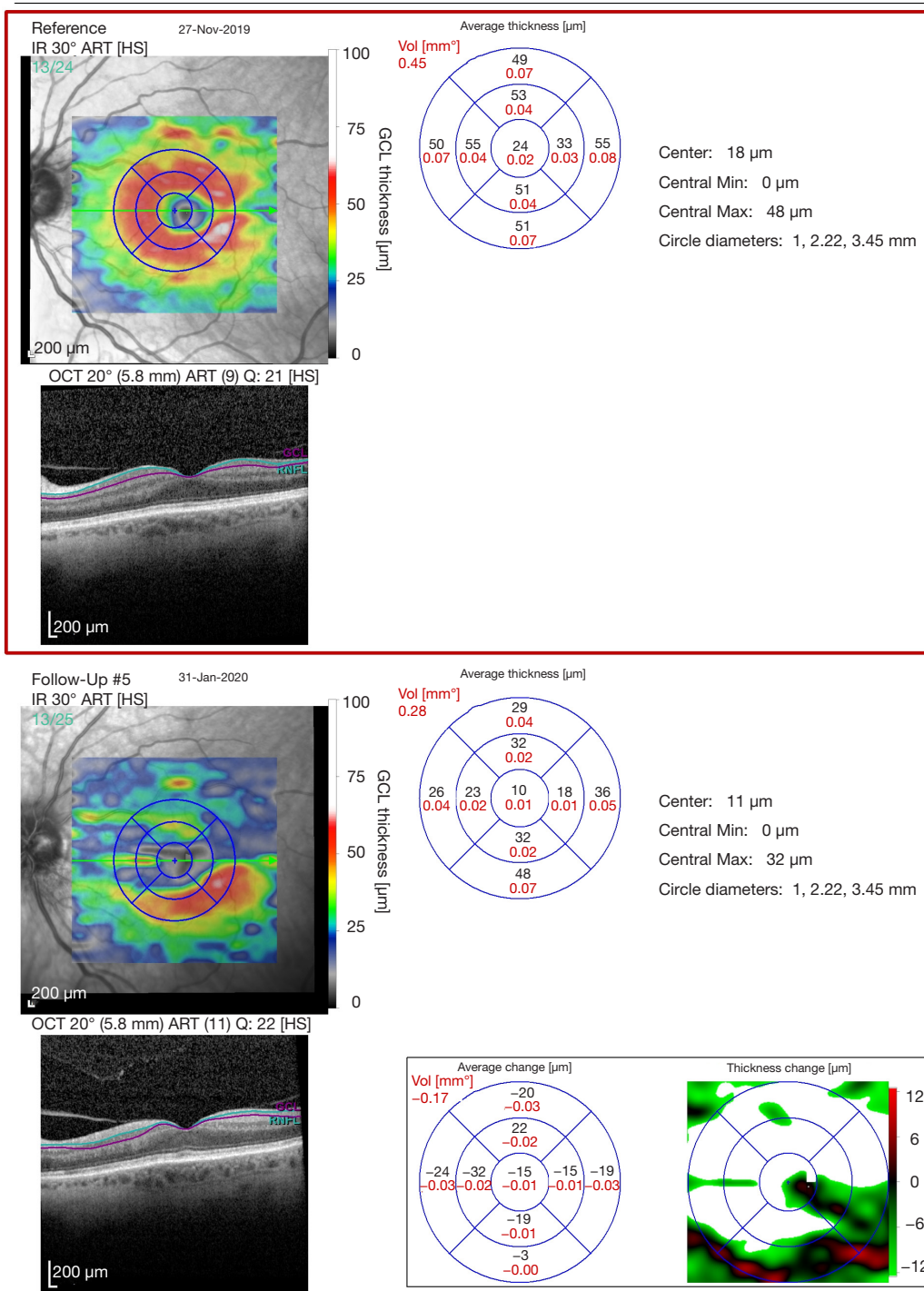
www.HeidelbergEngineering.com

Thickness Map Single Exam Report

Figure 5 Display software of mGCL density SD-OCT segmentation analysis (1, 2.22, 3.45 mm volume scan) of 28-year-old female with optic atrophy secondary to Leber hereditary optic neuropathy (LHON). The average mGCL thickness is diffusely reduced. mGCL, macular ganglion cell layer; SD-OCT, Spectral-domain optical coherence tomography.

is in keeping with the subjective and objective visual field loss, which in itself can aid in the diagnosis. For instances, in cases of compressive chiasmal compression, the pattern correlates with the bitemporal hemianopic defect in most cases. In cases of non-arteritic anterior ischemic optic neuropathy (NA-AION), the mGCIPL thinning mirrors the visual field deficit, which present often as altitudinal defects (*Figure 6*).

Besides its diagnostic value, assessment of the mGCIPL is also useful in serial monitoring of patients. Documented progression on OCT of ganglion cell loss in patients with documented mGCIPL thinning should prompt further assessment on possible causative mechanisms, in a fashion that is more reliable than serial perimetric assessment. For instance, in Leber hereditary optic neuropathy (LHON), mGCL thinning has been shown to precede visual loss,



Software Version: 6.9.5

www.HeidelbergEngineering.com

Thickness Map Change Report, Recent Follow-Up

Figure 6 Display software of serial mGCL density SD-OCT segmentation analysis (1, 2.22, 3.45 mm volume scan) in a patient with altitudinal inferior visual field loss secondary to a previous NA-AION. The superior mGCL is significantly reduced. The average volume change shows no significant progression. mGCL, macular ganglion cell layer; NA-AION, non-arteritic anterior ischemic optic neuropathy; SD-OCT, spectral-domain optical coherence tomography.

while in the acute stages, the pRNFL is increased in thickness. Therefore, assessment of the mGCL in a clinical scenario where the pRNFL is thickened should raise the suspicion of LHON (43).

Considerations when assessing pRNFL and GCL measurements

Physicians should be aware of the limitations inherent to automated GCL and pRNFL segmentation scans, taking these into account to minimize erroneous assessment and interpretation errors.

Automated segmentation may be affected by the quality of the OCT image, below the acceptable range stated by the OCT manufacturer (44). This should be considered when examining individuals in whom the image quality is poor, for example due to media opacities.

The center of the fovea that is assumed by the OCT software does not always correspond to the retinal locus of fixation (45,46), with deviations of approximately 60 ± 50 μm between fixation and the center of the foveal avascular zone (47). In some cases, manual location of the fixation point for foveal thickness measurements should be performed in order to correlate some measure of visual function at fixation with macular structure at the corresponding retinal locus (37).

OCT segmentation software algorithm automatically detects the pRNFL and GCL. In some cases, particularly in eyes with ocular pathology, the software incorrectly detects the correct boundary of the RNFL and GCL. In these cases, it might be more appropriate to manually correct the boundaries, which has been shown to have good inter-observer repeatability (37). The use of the eye tracker and retest software application has been shown to improve the reproducibility of RNFL measurements (48).

Repeatability of automated segmentation measurements has been demonstrated to differ across OCT devices and employed scan protocol (49). It is thus paramount to monitor patients using a constant method and similar OCT device. Furthermore, ocular pathology and low vision affects fixation and secondary measurement variability which could be misinterpreted as true clinical progression (50). Likewise, caution should be exerted when assessing retinal thickness changes occurring away from the immediate foveal zone (51).

Finally, in GCL analysis, the assessor should be familiar with the inner and outer retinal morphology of the macula. The individual inner and outer retinal layers appear to be symmetrical at low eccentricities, whereas at 5° eccentricity,

significant differences are found in the thickness of RNFL, GCL, INL, ONL and IRL.

Advances in OCT

SS-OCT

SS-OCT, a form of Fourier domain technology, obtains time-encoded spectral information by sweeping a narrow-bandwidth laser through a broad optical spectrum. Compared to SD-OCT, SS-OCT is less prone to signal attenuation along the axial path which in turn results in better image quality along the axial path. Tissue penetration is a major advantage of SS-OCT systems, due to the use of a light source less sensitive to scattering, centered at a $\sim 1,050$ -nm wavelength in contrast to ~ 840 nm in SD-OCT. Visualization of deep structures such as the choroid (52-65) and lamina cribrosa (66-70) is thus enhanced. Increased scanning speed results in a shorter scanning time and reduction in motion artefacts.

In neuro-ophthalmology, SS-OCT has been applied in the visualization and characterization of patients with ODD and in the differentiation between pseudo-papilledema and papilledema (71-73). It has also revealed important insights regarding the anatomy of the lamina cribrosa and microstructural changes incurred upon RNFL thinning and secondary visual field loss (74).

OCTA in neuro-ophthalmology

OCTA is a relatively recent OCT-based method that is increasingly being used in the assessment of patients with retinal vascular pathology. The use of OCTA in clinical neuro-ophthalmology remains limited, however, this is expected to change as the technique becomes more capable of providing pathophysiological explanations for some of the unanswered research and clinical questions in the field of vascular neuro-ophthalmic diseases.

OCTA images are motion-contrast images that rely on the variable backscattering of light from the vascular and neurosensory tissue in the retina. The inherent movement of the tissue dictates the intensity and phase of backscattered light from retinal tissue changes. Repeated scans are performed at the same location in order to differentiate moving particles from static tissue and the ensuing temporal changes of the OCT signal caused by these moving particles generate the angiographic contrast. OCTA employs two

methods for motion detection: amplitude decorrelation or phase variance. Amplitude decorrelation detects differences in amplitude between two different OCT B-scans. Phase variance is related to the emitted light wave properties, and the variation of phase when it intercepts moving objects. In retinal tissue, most movement is generated by red blood cells. After Fourier transform, the OCT signal contains amplitude (intensity) and phase information. Different components of the OCT signal are then devised by Fourier transform. They can be separated into three categories: phase-signal-based OCTA, intensity-signal-based OCTA, and complex-signal-based OCTA. Two averaging methods are applied to reduce background noise from normal eye movements, the split spectrum amplitude decorrelation technique and volume averaging. These OCTA algorithms produce an image (3 to 12 mm²) that is segmented into four zones: the superficial retinal plexus (including the superficial radial peripapillary capillaries and inner vascular plexus within the GCL), the deep retinal plexus, the outer retina, and the choriocapillaris (75). A detailed description of the principles of OCTA is beyond the scope of the article but can be found in other sources (76).

The resolution and detail of the *in vivo* vascular network images produced by OCTA approach those of histological samples. Significant advances in the understanding of the retinal vasculature have been made based on OCTA findings. In neuro-ophthalmology, OCTA assessment of peripapillary radial capillary network is particularly relevant, considering this is not visualized on fluorescein angiography (77). Peripapillary radial vessels are located in the RNFL, superficial to the 3D network of capillaries within the inner retina. In humans, these capillaries are known to stem from circumpapillary arterioles and not from vessels within the disc. They are particularly susceptible to fluctuations in intraocular pressure (IOP) and correlate with RNFL thickness (78). *Figure 7* exemplifies the OCTA analysis display in a healthy subject.

As expected, most studies on ONH microcirculation used glaucomatous optic neuropathy as a disease model. Indeed, reduced perfusion and reduced vessel density of the full-thickness ONH have been found to correlate with RNFL, ganglion cell complex, visual field mean deviation, and visual field index (79). A different approach assesses the pre-laminar blood flow, and takes into account the contribution of vessel area to the flow index of the ONH, the so-called normalized flux (80). The peripapillary (capillary) microcirculation is less prone to artefacts from large blood vessels and ONH structural variation and thus many studies described changes in flow and density with

progressive glaucomatous damage. It remains unanswered whether this occurs secondary to the loss of ganglion cells or whether microcirculation changes could be used to demonstrate early reversible changes that if left untreated will lead to downstream ganglion cell loss.

In neuro-ophthalmology, numerous studies have emerged in which OCTA is applied in cases of ischemic, inflammatory and inherited optic neuropathies. Reduced perfusion has been found in MSON patients when compared to MSNON and healthy controls (81). ONH and peripapillary microcirculation reduction has been shown in patients with NA-AION (82,83). In these patients, only the peripapillary microcirculation correlated with pRNFL and visual field deficit. Improvement in visual function has been found to be associated with partial recovery of peripapillary vascular flow, suggesting a possible clinical application of OCTA to monitor visual recovery in NA-AION patients (84). In acute arteritic anterior ischemic optic neuropathy (A-AION), dilation of the superficial peripapillary capillaries has been described as a non-specific sign, possibly due to short posterior ciliary arterial compromise resulting in luxury perfusion or hyperperfusion, or decreased optic nerve perfusion leading to centrally-mediated autoregulatory mechanisms. Focal non-perfusion of superficial and deep retinal capillaries has also been reported in A-AION. The combination of focal non-perfusion coupled with superficial peripapillary capillary dilation on OCTA may provide diagnostic clues when assessing patients with suspected A-AION (85). In eyes with optic atrophy secondary to prior papilledema (86) reduction in peripapillary microcirculation was observed in keeping with the observed pRNFL loss. In LHON and autosomal dominant optic atrophy (ADOA), reduction in peripapillary perfusion is observed in established cases as well as the typical telangiectatic changes seen in acute cases of LHON (87-92).

Adaptive optics OCT (AO-OCT)

AO is a technique that measures and corrects ocular aberrations in real time using a deformable mirror. Bypassing ocular imperfections across a dilated pupil, to minimize diffraction, results in an unprecedented lateral resolution (2–3 μm), enabling the visualization of individual cells *en face*. This technique has become a valuable ophthalmic research tool, and it is expected that further developments will ultimately result in its widespread use in the clinical setting.

The gain in axial resolution when AO is combined

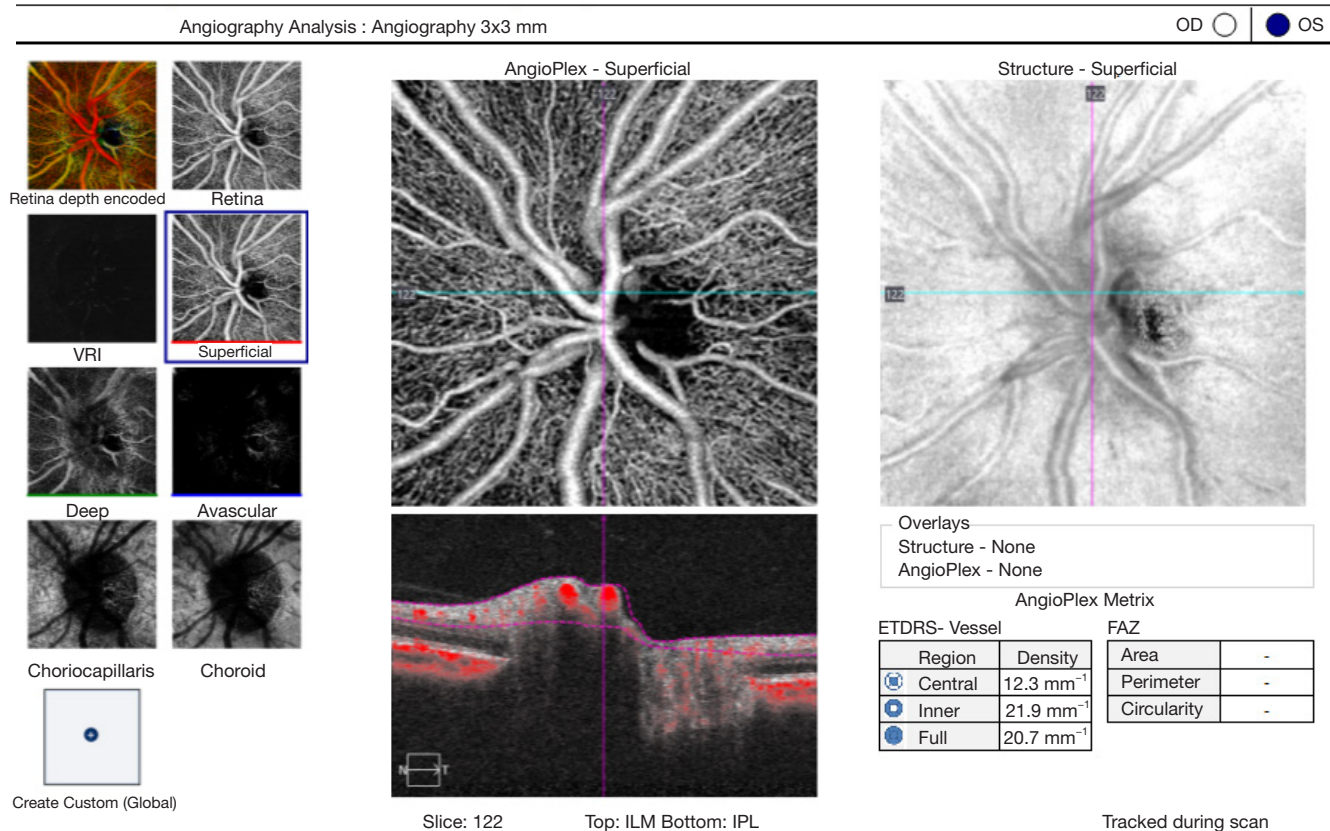


Figure 7 Display software of OCTA (3×3 mm) analysis of superficial vascular plexus of optic nerve head in a healthy subject acquired by Zeiss Cirrus HD-OCT 5000 (Zeiss Meditec, Dublin, CA, USA) with Angioplex. OCTA, optical coherence tomography angiography.

with OCT, AO-OCT, renders a new way of studying the 3D microscopic structure of the retina, with reduced speckle size and increased sensitivity to weak reflections. AO-OCT combinations include time-domain *en face* (xy) flood-illumination OCT using an aerial charge-coupled device (CCD), time-domain tomographic scanning (xz) ultrahigh-resolution OCT, time-domain *en face* scanning OCT, high-resolution SD-OCT, ultrahigh-resolution SD-OCT and SS-OCT. A detailed description of the principles of AO-OCT is beyond the scope of the article but can be found in other sources (93).

Besides its widespread use in the field of retinal research, AO-OCT systems have been used to study optic neuropathies (94,95). AO-OCT allows the capture of volume images of structures that would otherwise only be visible with histology, such as the RNFL, microstructures in the GCL and Henle's fibre layer and the pores of the lamina cribrosa.

Conclusions

The capabilities and scope of OCT applied to neuro-ophthalmology are expanding at a steady pace. The implementation of OCT has revolutionized ophthalmology and undoubtedly neuro-ophthalmology will continue to benefit from continued application of OCT in neuro-ophthalmic research and in the clinical management of patients with neuro-ophthalmic disorders. Selecting the appropriate OCT technique depends on the specific clinical query. Despite the increasing technological advances, critical questioning of computer-generated information must be integrated into the clinical context. This is crucial for the correct interpretation of findings and optimization of diagnostic accuracy, so that OCT leads to a paradigm shift in the diagnosis and monitoring of neuro-ophthalmic diseases.

Acknowledgments

Funding: None.

Footnote

Provenance and Peer Review: This article was commissioned by the Guest Editors (Fiona Costello and Steffen Hamann) for the series “The Use of OCT as a Biomarker in Neuro-ophthalmology” published in *Annals of Eye Science*. The article has undergone external peer review.

Conflicts of Interest: Both authors have completed the ICMJE uniform disclosure form (available at <http://dx.doi.org/10.21037/aes.2019.12.08>). The series “The Use of OCT as a Biomarker in Neuro-ophthalmology” was commissioned by the editorial office without any funding or sponsorship. The authors have no other conflicts of interest to declare.

Ethical Statement: The authors are accountable for all aspects of the work in ensuring that questions related to the accuracy or integrity of any part of the work are appropriately investigated and resolved.

Open Access Statement: This is an Open Access article distributed in accordance with the Creative Commons Attribution-NonCommercial-NoDerivs 4.0 International License (CC BY-NC-ND 4.0), which permits the non-commercial replication and distribution of the article with the strict proviso that no changes or edits are made and the original work is properly cited (including links to both the formal publication through the relevant DOI and the license). See: <https://creativecommons.org/licenses/by-nc-nd/4.0/>.

References

- Huang D, Swanson EA, Lin CP, et al. Optical coherence tomography. *Science* 1991;254:1178-81.
- Fujimoto J, Huang D. Foreword: 25 Years of Optical Coherence Tomography. *Invest Ophthalmol Vis Sci* 2016;57:OCTi-OCTii.
- de Boer JF, Leitgeb R, Wojtkowski M. Twenty-five years of optical coherence tomography: the paradigm shift in sensitivity and speed provided by Fourier domain OCT [Invited]. *Biomed Opt Express* 2017;8:3248-80.
- Reznicek L, Klein T, Wieser W, et al. Megahertz ultra-wide-field swept-source retina optical coherence tomography compared to current existing imaging devices. *Graefes Arch Clin Exp Ophthalmol* 2014;52:1009-16.
- Spaide RF. Enhanced depth imaging optical coherence tomography of retinal pigment epithelial detachment in age-related macular degeneration. *Am J Ophthalmol* 2009;147:644-52.
- Wong IY, Koizumi H, Lai WW. Enhanced depth imaging optical coherence tomography. *Ophthalmic Surg Lasers Imaging* 2011;42 Suppl:S75-84.
- Margolis R, Spaide RF. A pilot study of enhanced depth imaging optical coherence tomography of the choroid in normal eyes. *Am J Ophthalmol* 2009;147:811-5.
- Nishida Y, Fujiwara T, Imamura Y, et al. Choroidal thickness and visual acuity in highly myopic eyes. *Retina* 2012;32:1229-36.
- Usui S, Ikuno Y, Akiba M, et al. Circadian changes in subfoveal choroidal thickness and the relationship with circulatory factors in healthy subjects. *Invest Ophthalmol Vis Sci* 2012;53:2300-7.
- Spaide RF, Fujimoto JG, Waheed NK, et al. Optical coherence tomography angiography. *Prog Retin Eye Res* 2018;64:1-55.
- Spaide RF, Curcio CA. Evaluation of Segmentation of the Superficial and Deep Vascular Layers of the Retina by Optical Coherence Tomography Angiography Instruments in Normal Eyes. *JAMA Ophthalmol* 2017;135:259-62.
- Maloca PM, de Carvalho JER, Heeren T, et al. High-Performance Virtual Reality Volume Rendering of Original Optical Coherence Tomography Point-Cloud Data Enhanced With Real-Time Ray Casting. *Transl Vis Sci Technol* 2018;7:2.
- Maloca PM, Spaide RF, Rothenbuehler S, et al. Enhanced resolution and speckle-free three-dimensional printing of macular optical coherence tomography angiography. *Acta Ophthalmol* 2019;97:e317-9.
- Spaide RF. Volume-Rendered Optical Coherence Tomography of Diabetic Retinopathy Pilot Study. *Am J Ophthalmol* 2015;160:1200-10.
- Spaide RF. Volume-rendered angiographic and structural optical coherence tomography. *Retina* 2015;35:2181-7.
- Spaide RF, Klancnik JM Jr, Cooney MJ, et al. Volume-Rendering Optical Coherence Tomography Angiography of Macular Telangiectasia Type 2. *Ophthalmology* 2015;122:2261-9.
- Alonso R, Gonzalez-Moron D, Garcea O. Optical coherence tomography as a biomarker of neurodegeneration in multiple sclerosis: A review. *Mult Scler Relat Disord* 2018;22:77-82.

18. Merchant KY, Su D, Park SC, et al. Enhanced depth imaging optical coherence tomography of optic nerve head drusen. *Ophthalmology* 2013;120:1409-14.
19. Malmqvist L, Bursztyrn L, Costello F, et al. The Optic Disc Drusen Studies Consortium Recommendations for Diagnosis of Optic Disc Drusen Using Optical Coherence Tomography. *J Neuroophthalmol* 2018;38:299-307.
20. Yi K, Mujat M, Sun W, et al. Imaging of optic nerve head drusen: improvements with spectral domain optical coherence tomography. *J Glaucoma* 2009;18:373-8.
21. Murthy RK, Storm L, Grover S, et al. In-vivo high resolution imaging of optic nerve head drusen using spectral-domain Optical Coherence Tomography. *BMC Med Imaging* 2010;10:11.
22. Traber GL, Weber KP, Sabah M, et al. Enhanced Depth Imaging Optical Coherence Tomography of Optic Nerve Head Drusen: A Comparison of Cases with and without Visual Field Loss. *Ophthalmology* 2017;124:66-73.
23. Malmqvist L, Sibony PA, Fraser CL, et al. Peripapillary Ovoid Hyperreflectivity in Optic Disc Edema and Pseudopapilledema. *Ophthalmology* 2018;125:1662-4.
24. Karam EZ, Hedges TR. Optical coherence tomography of the retinal nerve fibre layer in mild papilloedema and pseudopapilloedema. *Br J Ophthalmol* 2005;89:294-8.
25. Sibony P, Strachovsky M, Honkanen R, et al. Optical coherence tomography shape analysis of the peripapillary retinal pigment epithelium layer in presumed optic nerve sheath meningiomas. *J Neuroophthalmol* 2014;34:130-6.
26. Pilat A, Sibley D, McLean RJ, et al. High-Resolution Imaging of the Optic Nerve and Retina in Optic Nerve Hypoplasia. *Ophthalmology* 2015;122:1330-9.
27. Takkar B, Molla K, Venkatesh P. Swept-source optical coherence tomography of an optic disc melanocytoma: The importance of the hyperreflective foci. *Indian J Ophthalmol* 2018;66:140-2.
28. Lee KH, Kim SW, Kwon SS, et al. Microperimetry and spectral domain optical coherence tomography in myelinated retinal nerve fibers. *Int J Ophthalmol* 2016;9:170-2.
29. Pierro L, Cicinelli MV, Marco G, et al. Swept source optical coherence tomography of a vitreal pocket entrapped in myelinated retinal nerve fibers. *Int Ophthalmol* 2015;35:881-2.
30. Nourinia R, Behdad B, Montahaei T. Optical coherence tomography findings in a patient with myelinated retinal nerve fiber layer. *J Ophthalmic Vis Res* 2013;8:280-1.
31. Kanamori A, Escano MF, Eno A, et al. Evaluation of the effect of aging on retinal nerve fiber layer thickness measured by optical coherence tomography. *Ophthalmologica* 2003;217:273-8.
32. Vanburen JM. Trans-Synaptic Retrograde Degeneration in the Visual System of Primates. *J Neurol Neurosurg Psychiatry* 1963;26:402-9.
33. Petzold A. Retinal glymphatic system: an explanation for transient retinal layer volume changes? *Brain* 2016;139:2816-9.
34. Petzold A. Optical Coherence Tomography to Assess Neurodegeneration in Multiple Sclerosis. *Methods Mol Biol* 2016;1304:131-41.
35. Petzold A, Balcer LJ, Calabresi PA, et al. Retinal layer segmentation in multiple sclerosis: a systematic review and meta-analysis. *Lancet Neurol* 2017;16:797-812.
36. Clark KJ, Balciunas D, Pogoda HM, et al. In vivo protein trapping produces a functional expression codex of the vertebrate proteome. *Nat Methods* 2011;8:506-15.
37. Ctori I, Huntjens B. Repeatability of Foveal Measurements Using Spectralis Optical Coherence Tomography Segmentation Software. *PLoS One* 2015;10:e0129005.
38. Balk LJ, Cruz-Herranz A, Albrecht P, et al. Timing of retinal neuronal and axonal loss in MS: a longitudinal OCT study. *J Neurol* 2016;263:1323-31.
39. Martinez-Lapiscina EH, Arnow S, Wilson JA, et al. Retinal thickness measured with optical coherence tomography and risk of disability worsening in multiple sclerosis: a cohort study. *Lancet Neurol* 2016;15:574-84.
40. Saidha S, Syc SB, Durbin MK, et al. Visual dysfunction in multiple sclerosis correlates better with optical coherence tomography derived estimates of macular ganglion cell layer thickness than peripapillary retinal nerve fiber layer thickness. *Mult Scler* 2011;17:1449-63.
41. De Dompablo E, Garcia-Montesinos J, Munoz-Negrete FJ, et al. Ganglion cell analysis at acute episode of nonarteritic anterior ischemic optic neuropathy to predict irreversible damage. A prospective study. *Graefes Arch Clin Exp Ophthalmol* 2016;254:1793-800.
42. Petzold A, de Boer JF, Schippling S, et al. Optical coherence tomography in multiple sclerosis: a systematic review and meta-analysis. *Lancet Neurol* 2010;9:921-32.
43. Asanad S, Tian JJ, Frousiakis S, et al. Optical Coherence Tomography of the Retinal Ganglion Cell Complex in Leber's Hereditary Optic Neuropathy and Dominant Optic Atrophy. *Curr Eye Res* 2019;44:638-44.
44. Balasubramanian M, Bowd C, Vizzeri G, et al. Effect of image quality on tissue thickness measurements obtained with spectral domain-optical coherence tomography. *Opt Express* 2009;17:4019-36.

45. Putnam NM, Hofer HJ, Doble N, et al. The locus of fixation and the foveal cone mosaic. *J Vis* 2005;5:632-9.
46. El-Ashry M, Hegde V, James P, et al. Analysis of macular thickness in British population using optical coherence tomography (OCT): An emphasis on interocular symmetry. *Curr Eye Res* 2008;33:693-9.
47. Zeffren BS, Applegate RA, Bradley A, et al. Retinal Fixation Point Location in the Foveal Avascular Zone. *Invest Ophthalmol Vis Sci* 1990;31:2099-105.
48. Langenegger SJ, Funk J, Toteberg-Harms M. Reproducibility of Retinal Nerve Fiber Layer Thickness Measurements Using the Eye Tracker and the Retest Function of Spectralis SD-OCT in Glaucomatous and Healthy Control Eyes. *Invest Ophthalmol Vis Sci* 2011;52:3338-44.
49. Eriksson U, Alm A. Repeatability in and interchangeability between the macular and the fast macular thickness map protocols: a study on normal eyes with Stratus optical coherence tomography. *Acta Ophthalmologica* 2009;87:725-30.
50. Comyn O, Heng LZ, Ikeji F, et al. Repeatability of Spectralis OCT Measurements of Macular Thickness and Volume in Diabetic Macular Edema. *Invest Ophthalmol Vis Sci* 2012;53:7754-9.
51. Gilmore ED, Hudson C. Eccentricity and measurement variability and repeatability with the retinal thickness analyser. *Br J Ophthalmol* 2004;88:62-5.
52. Adhi M, Liu J, Qavi A, et al. Comparison of the Accuracy of Choroidal Thickness Measurements Using SD-OCT With and Without EDI and Swept Source OCT and Volumetric Analysis of the Choroid in Healthy Eyes. *Invest Ophthalmol Vis Sci* 2013;54:4867.
53. Adhi M, Liu JJ, Qavi AH, et al. Enhanced Visualization of the Choroido-Scleral Interface Using Swept-Source OCT. *Ophthalmic Surg Lasers Imaging Retina* 2013;44:S40-2.
54. Akil H, Al-Sheikh M, Falavarjani KG, et al. Choroidal thickness and structural glaucoma parameters in glaucomatous, preperimetric glaucomatous, and healthy eyes using swept-source OCT. *Eur J Ophthalmol* 2017;27:548-54.
55. Chandrasekera E, Chen FK, Wong E, et al. Discrepancies in Manual and Automated Choroidal Thickness Measurements Using the Topcon Swept-Source Dri Oct-1 Atlantis System in a Cohort of Patients with a Wide Range of Macular and Choroidal Disease. *Clin Exp Ophthalmol* 2014;42:105.
56. De Geronimo D, Parravano M, Oddone F, et al. Exploring retinal-choroidal characteristics using Swept Source-OCT in healthy and highly myopic eyes. *Invest Ophthalmol Vis Sci* 2014;55:3341.
57. Glodan AM, Waldstein SM, Gerendas B, et al. Choroidal thickness derived from full-volume segmentation: Comparison of spectral-domain OCT with enhanced depth imaging versus 1050nm swept source OCT. *Invest Ophthalmol Vis Sci* 2014;55:3345.
58. Grover S, Sambhav K, Shakir O, et al. Decrease in Choroidal Thickness in Patients with Retinitis Pigmentosa Out of Proportion to the Retinal Thickness by Swept Source OCT. *Invest Ophthalmol Vis Sci* 2015;56:3805.
59. Liu JJ, Grulkowski I, Kraus MF, et al. In vivo imaging of the rodent eye with swept source/Fourier domain OCT. *Biomed Opt Express* 2013;4:351-63.
60. Maloca P, Gyger C, Hasler PW. A pilot study to compartmentalize small melanocytic choroidal tumors and choroidal vessels with speckle-noise free 1050 nm swept source optical coherence tomography (OCT choroidal "tumoropsy"). *Graefes Arch Clin Exp Ophthalmol* 2016;254:1211-9.
61. Xiong S, He X, Deng J, et al. Choroidal Thickness in 3001 Chinese Children Aged 6 to 19 Years Using Swept-Source OCT. *Sci Rep* 2017;7:45059.
62. Xu J, Li YD, Song SZ, et al. Evaluating changes of blood flow in retina, choroid, and outer choroid in rats in response to elevated intraocular pressure by 1300 nm swept-source OCT. *Microvasc Res* 2019;121:37-45.
63. Zafar S, Siddiqui MR, Shahzad R. Comparison of choroidal thickness measurements between spectral-domain OCT and swept-source OCT in normal and diseased eyes. *Clin Ophthalmol* 2016;10:2271-6.
64. Zhang L, Abramoff MD, Waldstein SM, et al. Reproducibility of automated choroidal thickness measurements: swept-source OCT and spectral-domain OCT using enhanced depth imaging. *Invest Ophthalmol Vis Sci* 2014;55:4796.
65. Zhou H, Chu ZD, Zhang QQ, et al. Attenuation correction assisted automatic segmentation for assessing choroidal thickness and vasculature with swept-source OCT. *Biomed Opt Express* 2018;9:6067-80.
66. Kim YW, Jeoung JW, Girard MJA, et al. Positional and Curvature Difference of Lamina Cribrosa According to the Baseline Intraocular Pressure in Primary Open-Angle Glaucoma: A Swept-Source Optical Coherence Tomography (SS-OCT) Study. *PLoS One* 2016;11:e0162182.
67. Li D, Li TB, Paschalis EI, et al. Optic Nerve Head Characteristics in Chronic Angle Closure Glaucoma

- Detected by Swept-Source OCT. *Curr Eye Res* 2017;42:1450-7.
68. Seol BR, Jeoung JW, Kim YK, et al. Investigating the relationship between focal lamina cribrosa defects and myopia using swept-source optical coherence tomography (SS-OCT). *Invest Ophthalmol Vis Sci* 2014;55:905.
 69. Taniguchi E, Paschalis EI, Li DJ, et al. Prelaminar and Lamina Cribrosa Defects Detected by Swept Source OCT in Glaucoma Stratified by Visual Field Loss Pattern. *Invest Ophthalmol Vis Sci* 2015;56:2056.
 70. Taniguchi E, Sangal N, Paschalis EI, et al. Imaging the Lamina Cribrosa using Spectral Domain OCT Enhanced Depth Imaging and Swept Source OCT in Open Angle Glaucoma Patients. *Invest Ophthalmol Vis Sci* 2014;55:900.
 71. Rebolleda G, Kawasaki A, de Juan V, et al. Optical Coherence Tomography to Differentiate Papilledema from Pseudopapilledema. *Curr Neurol Neurosci Rep* 2017;17:74.
 72. Ahn M, Eller AW, Wang B, et al. Imaging of optic disc drusen: Swept-Source (SS)-OCT versus B-scan ultrasound. *Invest Ophthalmol Vis Sci* 2015;56:3872.
 73. Silverman AL, Tatham AJ, Medeiros FA, et al. Assessment of optic nerve head drusen using enhanced depth imaging and swept source optical coherence tomography. *J Neuroophthalmol* 2014;34:198-205.
 74. Nadler Z, Wang B, Wollstein G, et al. Automated lamina cribrosa microstructural segmentation in optical coherence tomography scans of healthy and glaucomatous eyes. *Biomed Opt Express* 2013;4:2596-608.
 75. Chwalisz BK, Bouffard MA, Prasad S, et al. Neuroimaging diagnostic and monitoring approaches in ophthalmology. *Curr Opin Neurol* 2018;31:66-73.
 76. Kashani AH, Chen CL, Gahm JK, et al. Optical coherence tomography angiography: A comprehensive review of current methods and clinical applications. *Prog Retin Eye Res* 2017;60:66-100.
 77. Matsunaga D, Yi J, Puliafito CA, et al. OCT Angiography in Healthy Human Subjects. *Ophthalmic Surg Lasers Imaging Retina* 2014;45:510-5.
 78. Mase T, Ishibazawa A, Nagaoka T, et al. Radial Peripapillary Capillary Network Visualized Using Wide-Field Montage Optical Coherence Tomography Angiography. *Invest Ophthalmol Vis Sci* 2016;57:OCT504-10.
 79. L ev eque PM, Z eboulon P, Brasnu E, et al. Optic Disc Vascularization in Glaucoma: Value of Spectral-Domain Optical Coherence Tomography Angiography. *J Ophthalmol* 2016;2016:6956717.
 80. Bojikian KD, Chen CL, Wen JC, et al. Optic disc perfusion in eyes with primary open angle glaucoma and normal tension glaucoma using optical coherence tomography-based microangiography. *PLoS One* 2016;11:e0154691.
 81. Wang X, Jia YL, Spain R, et al. Optical coherence tomography angiography of optic nerve head and parafovea in multiple sclerosis. *Br J Ophthalmol* 2014;98:1368-73.
 82. Hata M, Oishi A, Muraoka Y, et al. Structural and Functional Analyses in Nonarteritic Anterior Ischemic Optic Neuropathy: Optical Coherence Tomography Angiography Study. *J Neuroophthalmol* 2017;37:140-8.
 83. Rebolleda G, Diez-Alvarez L, Marin YG, et al. Reduction of Peripapillary Vessel Density by Optical Coherence Tomography Angiography from the Acute to the Atrophic Stage in Non-Arteritic Anterior Ischaemic Optic Neuropathy. *Ophthalmologica* 2018;240:191-9.
 84. Sharma S, Ang M, Najjar RP, et al. Optical coherence tomography angiography in acute non-arteritic anterior ischaemic optic neuropathy. *Br J Ophthalmol* 2017;101:1045-51.
 85. Gaier ED, Gilbert AL, Cestari DM, et al. Optical coherence tomographic angiography identifies peripapillary microvascular dilation and focal non-perfusion in giant cell arteritis. *Br J Ophthalmol* 2018;102:1141-6.
 86. Ghasemi Falavarjani K, Tian JJ, Akil H, et al. Swept-source optical coherence tomography angiography of the optic disk in optic neuropathy. *Retina* 2016;36 Suppl 1:S168-77.
 87. Balducci N, Cascavilla ML, Ciardella A, et al. Peripapillary vessel density changes in Leber's hereditary optic neuropathy: a new biomarker. *Clin Exp Ophthalmol* 2018;46:1055-62.
 88. De Rojas JO, Rasool N, Chen RWS, et al. Optical coherence tomography angiography in Leber hereditary optic neuropathy. *Neurology* 2016;87:2065-6.
 89. Gaier ED, Gittinger JW, Cestari DM, et al. Peripapillary Capillary Dilation in Leber Hereditary Optic Neuropathy Revealed by Optical Coherence Tomographic Angiography. *JAMA Ophthalmol* 2016;134:1332-4.
 90. Kousal B, Kolarova H, Meliska M, et al. Peripapillary microcirculation in Leber hereditary optic neuropathy. *Acta Ophthalmologica* 2019;97:e71-6.
 91. Takayama K, Ito Y, Kaneko H, et al. Optical coherence tomography angiography in leber hereditary optic neuropathy. *Acta Ophthalmologica* 2017;95:e344-5.

92. Martins A, Rodrigues TM, Soares M, et al. Peripapillary and macular morpho-vascular changes in patients with genetic or clinical diagnosis of autosomal dominant optic atrophy: a case-control study. *Graefes Arch Clin Exp Ophthalmol* 2019;257:1019-27.
93. Miller DT, Kocaoglu OP, Wang Q, et al. Adaptive optics and the eye (super resolution OCT). *Eye (Lond)* 2011;25:321-30.
94. Choi SS, Zawadzki RJ, Keltner JL, et al. Changes in cellular structures revealed by ultra-high resolution retinal imaging in optic neuropathies. *Invest Ophthalmol Vis Sci* 2008;49:2103-19.
95. Choi SS, Zawadzki RJ, Lim MC, et al. Evidence of outer retinal changes in glaucoma patients as revealed by ultrahigh-resolution in vivo retinal imaging. *Br J Ophthalmol* 2011;95:131-41.

doi: 10.21037/aes.2019.12.08

Cite this article as: de Carvalho ER, Maloca PM. Overview of optical coherence tomography in neuro-ophthalmology. *Ann Eye Sci* 2020;5:14.